IOPscience iopscience.iop.org

Home Search Collections Journals About Contact us My IOPscience

Tiling theory applied to the surface structure of icosahedral AlPdMn quasicrystals

This article has been downloaded from IOPscience. Please scroll down to see the full text article.

1999 J. Phys.: Condens. Matter 11 2729

(http://iopscience.iop.org/0953-8984/11/13/010)

View the table of contents for this issue, or go to the journal homepage for more

Download details:
IP Address: 171.66.16.214
The article was downloaded on 15/05/2010 at 07:16

Please note that terms and conditions apply.

J. Phys.: Condens. Matter **11** (1999) 2729–2748. Printed in the UK PII: S0953-8984(99)95374-2

Tiling theory applied to the surface structure of icosahedral AlPdMn quasicrystals

Peter Kramer, Zorka Papadopolos and Harald Teuscher
Institut für Theoretische Physik der Universität Tübingen, Germany

Received 26 June 1998, in final form 30 November 1998

Abstract. Surfaces of i-$Al_{68}Pd_{23}Mn_9$ as observed in scanning tunnelling microscopy (STM) and low-energy electron diffraction (LEED) experiments show atomic terraces in a Fibonacci spacing. We analyse them in a bulk tiling model due to Elser which incorporates many experimental data. The model has dodecahedral Bergman clusters within an icosahedral tiling $\mathcal{T}^{*(2F)}$ and is projected from the six-dimensional face-centred hypercubic lattice. We derive the occurrence and Fibonacci spacing of atomic planes perpendicular to any fivefold axis, compute the variation of planar atomic densities, and determine the (auto-) correlation functions. Upon interpreting the planes as terraces at the surface, we find quantitative agreement with the STM experiments.

1. Introduction

The bulk structure of the icosahedral phases i-AlPdMn, i-AlFeCu and their modelling in terms of a six-dimensional (6D) description has been an active research field for more than a decade. Of the many papers on this topic, we mention only a few. Many more references are quoted in these publications. Katz and Gratias [7] derive from previous work for i-AlFeCu a quasiperiodic network of atomic positions. It is generated by three basic atomic windows related to the 6D hypercubic F-lattice. They examine the interatomic distances carefully. de Boissieu *et al* [2] determine for i-AlPdMn from x-ray and neutron data in detail the decomposition of the atomic surfaces. All of these models use the 6D embedding, and the parallel and the perpendicular space. Elser [4] generalizes and unifies these two models and interprets them in terms of clusters occupying the odd and even vertices of the icosahedral tiling related to the 6D hypercubic P-lattice: the odd vertices form the centres of Bergman clusters, which then build up Mackay clusters around the even vertices. Additional atomic positions are related to this basic structure. The Elser model was actually created for the study of random tilings, but by construction admits a perfect tiling structure which then incorporates the main experimental data which have led to the models given by Katz and Gratias and by de Boissieu *et al*. As shown in [11], the Elser model can be taken as a *network of atomic positions in a tiling model*, denoted by $\mathcal{T}^{*(2F)}$ and related to the observed hypercubic F-lattice and module. This tiling model will be used in what follows. Its composite atomic surfaces are closely related to those of the Katz–Gratias model [7].

The surface structure of i-$Al_{68}Pd_{23}Mn_9$ perpendicular to the fivefold axes has been explored by various groups. Schaub *et al* [15] applied scanning tunnelling microscopy (STM) and low-energy electron diffraction (LEED) to obtain atomic-scale information for a sputtered and annealed surface. They observed a sequence of 11 atomically flat terraces. Two spacings of 4.22 ± 0.26 and 6.78 ± 0.24 Å form a Fibonacci string of the type LLSLLSLSLL. Pentagonal

0953-8984/99/132729+20$19.50 © 1999 IOP Publishing Ltd

holes of a single fixed orientation appear within these terraces. Gierer *et al* [5,6] by dynamical LEED studies for a similarly prepared surface confirm the quasicrystalline structure. To interpret their data they perform dynamical diffraction calculations for assumed terminations of a model patch from the bulk model of de Boissieu *et al* [2]. They find optimal agreement for Al-rich terminations of high atomic density. A study by Ebert *et al* [3] of surfaces cleaved *in situ* revealed terraces only after the annealing of the initially rather rough surface.

For the theory of quasicrystals, the experiments raise the question of what quasiperiodic repetition pattern and what structure variation within planes can be rigorously obtained from a bulk model of i-$Al_{68}Pd_{23}Mn_9$. In the present paper we address these questions in the description using the tiling model. We develop a quasiperiodic analysis similar to that of crystal surfaces in terms of particular net-planes. To obtain exact results we cannot rely on features seen in a model patch. Instead we make full use of the technique of windows or coding for quasiperiodic structures. The general principles of the window technique have been described in several monographs on quasicrystals. We illustrate them for the well-known one-dimensional Fibonacci paradigm. We then apply the unique method of lifting and projection between the physical (parallel) and the window (perpendicular) space, called the star-map by Moody [14], to the icosahedral F-module, to the tiling, and to its decoration. It turns out that our main results can be expressed in terms of the one-dimensional Fibonacci system.

We now survey the model input and the content of the following sections. Our bare tiling model has the following data: we adopt the $\mathcal{T}^{*(2F)}$ tiling model projected from the face-centred hypercubic lattice (2F) $\sim D_6$ in E^6. Upon scaling by a factor of 2, the lattice (2F) comprises the *even-vertex points (index sum even)* of the full hypercubic P-lattice whose projection was given in [9]. For a full description of the tiling and its projection we refer the reader to [10]. Its vertex points are projected lattice points. We shall use two units of length: ⑤ is the length along fivefold axes of the six basis vectors e_i, $i = 1, \ldots, 6$, of the hypercubic lattice, projected onto one of the two invariant icosahedral subspaces, $E_\parallel$ or $E_\perp$. Along the projected twofold axes, we choose the standard length ② $= (2/\sqrt{\tau+2})$⑤. To convert to atomic distances in i-AlPdMn, we adopt from [4, 11] the τ-scaled short-edge length of the tiling:

$$s = \tau ② = \frac{2\tau}{\sqrt{\tau+2}} ⑤ \qquad ⑤ \to 4.56 \text{ Å}. \tag{1}$$

The window of the vertex points for the tiling is in $E_\perp$ the triacontahedron [8, 10] shown in figure 5—see later. The tiling is decorated according to Elser [4] with dodecahedral Bergman clusters [11]. The mid-points of these Bergman clusters are placed on the projected *odd-vertex points* of the hypercubic lattice. Their edge length is $\tau^{-1}② = 2.96$ Å and their height along a fivefold direction is $[(2\tau^2)/(\tau+2)]⑤ = 6.60$ Å. For all other atomic positions, most of which do not enter the present analysis, we refer the reader to [4, 11].

In section 2 we develop the window technique for the bulk tiling and its planes perpendicular to the fivefold axes. We start in subsection 2.1 with the Fibonacci tiling and explain the technique of windows. We briefly describe the icosahedral tiling $\mathcal{T}^{*(2F)}$ for the F-phase, subsection 2.2, and planes of vertex points perpendicular to a fivefold axis in a 3D space $E_\parallel$, subsection 2.3, and give their windows in $E_\perp$. We shift between these planes along Fibonacci lines, subsection 2.4, and show that most of the vertex points belong to a system of shifted planes, subsection 2.5. In subsection 2.6 we interpret the terraces found in the STM experiment as terminations of the bulk model. From the tiling model we prove the existence of a full Fibonacci sequence of planes and of a spacing as found in the STM experiment, and we predict variations of the density of vertex points along the sequence, with bounds from the observed Fibonacci string.

In section 3 we use the decoration of the tiling to infer more structure information for

within the planes from other atomic positions of the tiling model. In particular we look for pentagonal structures as seen in the STM experiments [15]. We consider the dodecahedral Bergman clusters of the Elser model [4] on the tiling. The dodecahedra have two pentagonal vertex sets of the same orientation perpendicular to a fivefold axis. The corresponding cutting planes are transformed in subsection 3.1 by lifting and projection to the perpendicular space. Their window description with respect to the triacontahedron is derived. The correlation with vertex points of the tiling gives rise to three alternative models for the structure within planes. The predicted density of vertex points and pentagons is derived in exact form in subsection 3.2. In subsection 3.3 we compute in closed form the Patterson function within planes for vertex points and pentagon centres.

The bulk structure of the tiling model, analysed here up to the level of Bergman clusters, displays for the planes a repetition and structure pattern in line with the terrace structure found in the experiments [15] which stimulated the present analysis. A complementary approach to the terrace structure, based on generating a model patch, is given in [12] and confirms the present analysis.

2. Tilings and windows

2.1. Fibonacci lines, their windows, and the search for the string LLSLLSLSLL

We recall the well-known projection and window technique for the Fibonacci tiling $\mathcal{T}$. We shall emphasize the window technique since it will be needed when we apply Fibonacci lines to the icosahedral tiling in subsections 2.4–2.6. Let Λ be the square lattice in 2D whose edge length we adjust for convenience to $\sqrt{\tau+2}$, $\tau = \frac{1}{2}(1+\sqrt{5})$. In a lattice basis the points of Λ are

$$x = n_1 e_1 + n_2 e_2. \tag{2}$$

In a system of coordinates $(x_\parallel, x_\perp)$ rotated by ϕ with respect to the natural basis: $c = \cos(\phi) = \tau/\sqrt{\tau+2}$ and $s = \sin(\phi) = 1/\sqrt{\tau+2}$, the basis vectors are

$$e_1 = (c, -s)\sqrt{\tau+2} \qquad e_2 = (s, c)\sqrt{\tau+2} \tag{3}$$

and the coordinates of the lattice points become

$$\begin{aligned}(x_\parallel, x_\perp) &= (n_1 e_{1\parallel} + n_2 e_{2\parallel}, n_1 e_{1\perp} + n_2 e_{2\perp}) \\ &= (x_\parallel(n_1, n_2), x_\perp(n_1, n_2)) = (n_1\tau + n_2, -n_1 + n_2\tau).\end{aligned} \tag{4}$$

The projections $(x_\parallel, x_\perp)$ form two τ-modules on the orthogonal lines $E_\parallel$, $E_\perp$ respectively. There is a *unique map* $x_\parallel(n_1, n_2) \Leftrightarrow x_\perp(n_1, n_2)$ between these modules, corresponding to the star-map of Moody [14], and there is a *unique lifting* of $x_\parallel(n_1, n_2)$ or $x_\perp(n_1, n_2)$ to a point of Λ. The projections $x_\parallel(\Lambda)$, $x_\perp(\Lambda)$ cover $E_\parallel$, $E_\perp$ densely and uniformly.

Upon choosing in $E_\perp$ the *window* $f_\perp := (-1, \tau]$, whose length $|w_\perp| = \tau + 1$ is the projection of a unit square to $E_\perp$, the vertex set of the Fibonacci tiling $\mathcal{T}$ in $E_\parallel$ is defined as

$$v(\mathcal{T}) = \{x_\parallel(n_1, n_2) | x_\perp(n_1, n_2) \in f_\perp\}. \tag{5}$$

The end-points of the window are restricted in order to avoid ambiguities. When $\mathcal{T}$ is lifted back into $\Lambda \in E^2$, it forms the vertex set of a continuous staircase formed by edge lines as shown in figure 1.

The projections of the steps to $E_\parallel$ form the familiar Fibonacci tiling with two tiles S, T of length 1, τ respectively. With $x_\parallel$ increasing, adjacent tiles form the vertex configurations

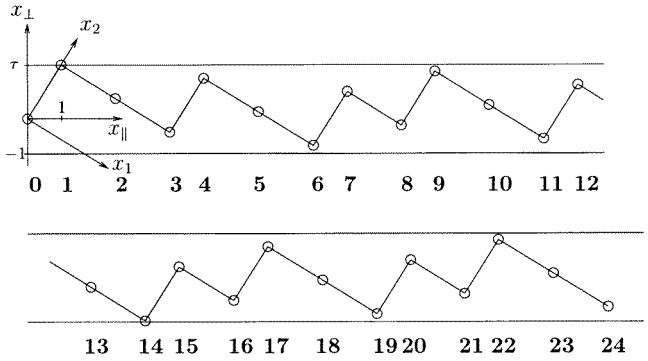

Figure 1. The Fibonacci tiling is the projection of a staircase, formed by edge lines in a square lattice, to a line $E_\parallel$ of slope τ^{-1}. The successive vertices $x_\parallel$ of the staircase may be enumerated by the single integer $N = n_1 + n_2$. Projected to $x_\parallel$, the edge lines form the Fibonacci tiling with two tiles S, L of length 1, τ respectively. The projections $x_\perp(N)$ of the vertices to the orthogonal space $E_\perp$ fall into a window $f_\perp = (-1, \tau]$ of length $\tau + 1$.

LS, LL or LS. The windows in $E_\perp$ for these vertex configurations can be shown to form subwindows of $f_\perp$ given by

$$\begin{aligned} f_\perp^{LS} &= (-1, 0] \\ f_\perp^{LL} &= (0, \tau - 1] \\ f_\perp^{SL} &= (\tau - 1, \tau]. \end{aligned} \tag{6}$$

We now wish to compare and analyse Fibonacci tilings with different starting points. Because of the uniform dense covering, we may choose in $E_\perp$ an arbitrary initial point $c_\perp \in w_\perp$ and associate with it an initial point of a tiling $\mathcal{T}(c_\perp)$. We label the initial vertex by $(0, 0) \Rightarrow 0$ and the successive vertices of $\mathcal{T}(c_\perp)$ by the single integer $N = n_1 + n_2$. From the window condition we can generate $x_\parallel(N), x_\perp(N)$ step by step according to

$$\begin{aligned} x_\perp(N+1) &= \begin{bmatrix} x_\perp(N) - 1 \leftrightarrow (x_\perp(N) - 1) \in f_\perp \\ x_\perp(N) + \tau \leftrightarrow (x_\perp(N) + \tau) \in f_\perp \end{bmatrix} \\ x_\parallel(N+1) &= \begin{bmatrix} x_\parallel(N) + \tau \\ x_\parallel(N) + 1. \end{bmatrix} \end{aligned} \tag{7}$$

The steps in $E_\parallel$ propagate the tiling by adding a new tile L or S. For later purposes, like in the determination of densities of points in subsection 3.2, we emphasize the propagation as a function of N in terms of the perpendicular coordinate in the window.

We adjust the perpendicular coordinate to the mid-point of the window and scale it by a factor τ to obtain the new variable

$$y_\perp(N) := \tau x_\perp(N) - \tfrac{1}{2} \tag{8}$$

whose window $w_\perp = (-\frac{1}{2}\tau^3, \frac{1}{2}\tau^3]$ now has the length $|w_\perp| = \tau^3$ with the central subwindow for LL vertex configurations of length $|w_\perp^{LL}| = 1$. It can be shown that the subset of LL vertices of the original tiling form another Fibonacci vertex set scaled by a factor τ^3. The function $y_\perp(N)$ is plotted in figure 2 for four initial values from the subwindow $w_\perp^{LL}$. This figure illustrates the variety of sequences as a function of the initial value. Successive values are connected by straight lines. The reason for starting at an LL subwindow will become apparent when we go to the icosahedral tiling in subsection 2.4.

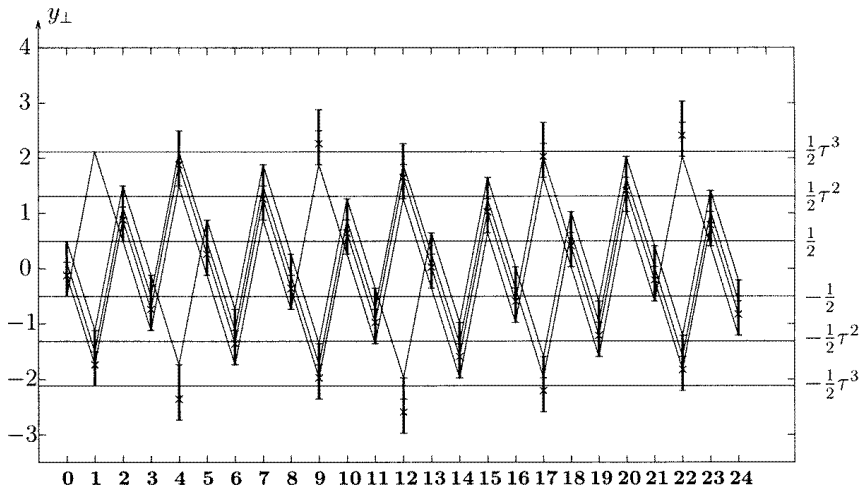

Figure 2. Four Fibonacci lines starting at an LL vertex are coded by four initial points in a vertical subwindow scaled by τ^{-3}. The vertical coordinate is $y_\perp(N)$ of equation (8). For steps numbered from 0 to 24, the lines connect the images in the window for these four points. Each step produces in $E_\parallel$ a long or short interval of the corresponding Fibonacci line.

With the window technique we search for the finite string LLSLLSLSLL found in the terrace spacing of the experiment [15]. For a Fibonacci line coded by the initial point $y_\perp(0) = -\frac{1}{2}$, this string occurs at the points $N = 9, \ldots, 19$; compare figures 2 and 6 (see later). For other initial points, the string would occur at some other step. We infer all possible occurrences of the string as conditions with respect to the window: the string will be stable under vertical shifts $\Delta y_\perp(0)$ of the initial point as long as its highest value $y_\perp(17)$ and its lowest value $y_\perp(14)$ do not pass the limits $\pm\frac{1}{2}\tau^3$ respectively of the window $w_\perp$. These window conditions are independent of the initial point. Clearly the appearance of the string puts narrow bounds on the corresponding values of $y_\perp$; compare subsection 2.6.

2.2. Icosahedral tilings

The construction of 3D tilings follows the paradigm given by the Fibonacci line. The projections are now determined by requiring non-crystallographic and in particular icosahedral point symmetry after projection. It is well known that an icosahedral tiling $\mathcal{T}^{\mathrm{P}}$ with two rhombohedral tiles arises by icosahedral projection to 3D from the primitive hypercubic P-lattice and module in 6D [9].

In two orthogonal 3D spaces $E_\parallel$, $E_\perp$, we find the six fivefold, ten threefold and fifteen twofold axes associated with the icosahedral group. The six primitive basis vectors $e_1, \ldots, e_6$ of the hypercubic lattice upon projection point along fivefold axes. Their length we denote by ⑤, and their directions we choose as follows [10]: in $E_\parallel$ we take $\cos(e_{1\parallel}, e_{i\parallel}) = 1/\sqrt{\tau+2}$, $i = 2, \ldots, 6$, and for $i = 2, \ldots, 5$ pass from $e_{i\parallel}$ to $e_{i+1\parallel}$ by a rotation around $e_{1\parallel}$ with angle $2\pi/5$. In $E_\perp$ we take $\cos(e_{1\perp}, e_{i\perp}) = -1/\sqrt{\tau+2}$, $i = 2, \ldots, 6$, and for $i = 2, \ldots, 5$ pass from $e_{i\perp}$ to $e_{i+1\perp}$ by a rotation around $e_{1\perp}$ with angle $4\pi/5$. All vectors along twofold axes arise from projections of $(e_i \pm e_j)$, $i \neq j$. Their shorter length we denote by ② $= (2/\sqrt{\tau+2})$⑤.

The icosahedral quasicrystals i-AlFeCu and i-AlPdMn are indexed from their diffraction pattern according to the hypercubic face-centred or F-lattice and -module rather than the primitive P-module. The hypercubic F-lattice, scaled by a factor of 2 and denoted here as (2F),

may be viewed as the subset of even lattice points (index sum even) from the full hypercubic lattice in 6D.

Turning our attention to this lattice and module, we briefly summarize the construction of the icosahedral tiling $\mathcal{T}^{*(2F)}$ associated with the F-lattice and given in [10]. In both 3D spaces we have 6D modules whose bases can be formed for example from three short and three long vectors along three selected twofold axes. Via the unique lifting and projection, there is a one-to-one map $q_\parallel \Leftrightarrow q_\perp$, the star-map of [14], between points $q_\parallel$ and $q_\perp$ of the two modules in $E_\parallel$ and $E_\perp$. For simplicity we suppress the basis and the six integers in $q_\parallel, q_\perp$ which generalize equation (4) and underlie this map. The vertex points of the tiling $\mathcal{T}^{*(2F)}$ are, as a generalization of equation (5), given by

$$v(\mathcal{T}^{*(2F)}) = \{q_\parallel | q_\perp \in \text{triacontahedron}\} \tag{9}$$

i.e. the projections $q_\parallel \in E_\parallel$ of those lattice points whose projections $q_\perp \in E_\perp$ fall into the triacontahedral window; compare figure 5, later. The projections $\{q_\perp\}$ fill the triacontahedron densely and uniformly. The triacontahedron is the icosahedral projection to $E_\perp$ of the Voronoi or Wigner–Seitz cell of the F-lattice in 6D. The tiling $\mathcal{T}^{*(2F)}$ has six tetrahedral tiles. In its present simple form, we need only two tetrahedra with threefold symmetry axes. The vertices of these two tetrahedra coincide with four even vertices of the two rhombohedra associated with the tiling $\mathcal{T}^{P}$. The simple form of the tiling $\mathcal{T}^{*(2F)}$ is fully described by putting atoms into positions on the full rhombohedral tiles but allowing for the distinction of even and odd vertices, as is done in the Elser model [4, 11]. We shall need only the even- and odd-vertex points.

The relationship of the tilings $\mathcal{T}^{*(2F)}$ and $\mathcal{T}^{P}$ may be summarized as follows: the triacontahedral windows for the vertex sets coincide. The modules differ from one another: the (2F) module is the even submodule of the P-module. By expanding each of the two threefold-symmetric tetrahedra back into the corresponding rhombohedron and dropping the distinction between even and odd vertices we can locally derive $\mathcal{T}^{P}$ from $\mathcal{T}^{*(2F)}$.

2.3. Planes perpendicular to fivefold axes

We turn to planes in the tiling $\mathcal{T}^{*(2F)}$. Fix in $E_\parallel$ a fivefold axis parallel to $e_{1\parallel}$ as in figure 4, later, and consider vertex points $q_\parallel$ in a plane perpendicular to it. Next we pass to $E_\perp$; consider the corresponding fivefold axis parallel to $e_{1\perp}$ and the images $q_\perp$ of the vertex points $q_\parallel$ from the plane under the one-to-one map. It turns out that these images $q_\perp \in E_\perp$ lie again in a plane perpendicular to the fivefold axis. In addition they must be points from the triacontahedron. Hence we get the following result:

Proposition 1. *The window for vertex points $q_\parallel$ from the tiling $\mathcal{T}^{*(2F)}$ in a fixed plane perpendicular to a fivefold axis is in $E_\perp$ the intersection of a plane perpendicular to the corresponding fivefold axis with the triacontahedron.*

The triacontahedron is shown in figure 5—see later—in a view perpendicular to a fivefold axis. The distance from the centre to a fivefold vertex is τ⑤, where ⑤ is the standard length along a fivefold axis. The triacontahedron with respect to this fivefold axis has a central decagonal prism of thickness $[2\tau^{-1}/(\tau + 2)]\tau$⑤. Kepler in 1619 [8] not only introduced the triacontahedron, but also visualized these decagonal prisms and denoted them by the letters Xx; see figure 3.

The central decagonal prism of the triacontahedron when seen as a subwindow for part of the tiling $\mathcal{T}^{*(2F)}$ has a particular significance, as is shown in [13]: any planar decagonal intersection of the triacontahedron in $E_\perp$ determines in $E_\parallel$ an infinite planar tiling TTT with

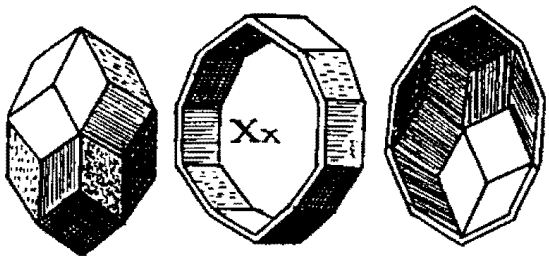

Figure 3. Kepler's decomposition of the triacontahedron into a central decagonal prism Xx and two shells.

two golden triangles; compare [1]. With respect to the full 3D tiling $\mathcal{T}^{*(2F)}$, this planar subtiling is formed by faces of tetrahedral tiles.

The planar intersections of the triacontahedron outside the decagonal prism are windows for planes of vertex points which in general do not form a planar tiling. From the uniform covering of the window it follows that the density of vertex points in all planes is proportional to the area of its window, i.e. of the corresponding intersection of the triacontahedron. We shall compute this density in subsection 3.2.

2.4. Fibonacci shifts between parallel planes

The planar TTT subtiling has the property that through any vertex point there passes at least one infinite Fibonacci line. In terms of its decagonal subwindow this results from the geometric property that any interior point belongs to at least one subwindow for an infinite Fibonacci line. In $E_\parallel$ this Fibonacci line points along a twofold axis associated with two vectors whose length scales by τ. All subwindows for a fixed Fibonacci line are sections of length $\tau^2$② on parallel lines perpendicular to and bounded by opposite rectangular faces of a decagonal prism.

As the initial plane we shall choose a reference plane whose vertex points form a triangle TTT pattern. All of these planes have the same highest density of vertex points; see subsection 3.2. To shift between planes perpendicular to a fixed fivefold axis, we shall use vectors along twofold axes outside this plane. From the orbit in $E_\parallel$ of the twofold axis with respect to the fivefold one, we pick two perpendicular twofold coplanar axes 2, 2′ which form with the 5-axis the angles $\arccos(1/\sqrt{\tau+2}) = 58.3^\circ$, $\arccos(\tau/\sqrt{\tau+2}) = 31.7^\circ$; see figure 4. In the notation of [10], we choose the axis 5 along $e_{1\parallel}$, the axis 2 along the short and long vectors $-(e_2+e_3)_\parallel$, $(e_1+e_5)_\parallel$, and the axis 2′ along the short and long vectors $(e_1+e_5)_\parallel$, $-(e_4+e_6)_\parallel$ respectively.

The vectors along the twofold axis 2 from equation (1) have the τ-scaled model lengths τ②, $\tau^2$②. By multiplication with the cosine of the corresponding angle we get the parallel spacings of planes perpendicular to the fivefold axis 5. These spacings become $[2\tau/(\tau+2)]$⑤ and $[2\tau^2/(\tau+2)]$⑤ respectively. By comparison, the two vectors along the twofold axis 2′ yield along the fivefold axis spacings scaled by a factor τ. Therefore the latter vectors will not generate additional parallel planes. We obtain the short and long spacings 4.08 and 6.60 Å respectively, fully in line with the terrace spacing observed in [15] and quoted in section 1. So we have identified in the bulk tiling model the shift vectors which generate the terrace structure.

To ensure that, starting from a fixed plane, we generate by shifts an infinite system of parallel planes, we turn to $E_\perp$. In $E_\perp$ the three axes 2, 2′, 5 remain coplanar but the directions

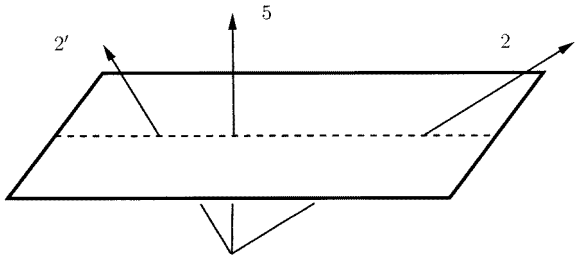

Figure 4. Two typical perpendicular twofold axes 2, 2′ can be chosen within a plane with a fivefold axis 5. A plane perpendicular to this axis can be shifted from the origin by vectors along these twofold axes.

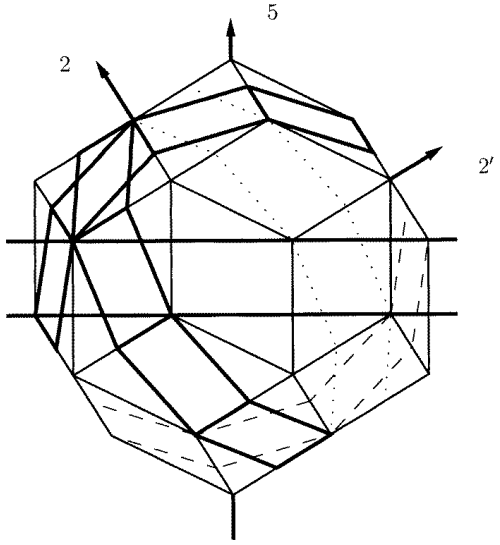

Figure 5. Three decagonal prisms of the triacontahedron in $E_\perp$: the first one has its fivefold axis 5 in the vertical direction. The second and third prism have opposite rectangular faces perpendicular to two twofold axes 2, 2′ coplanar with the axis 5.

and angles of 2 and 2′ are interchanged; see figure 5. We get infinite Fibonacci lines along the axes 2, 2′ if the vectors along these axes can be associated with decagonal prisms of the triacontahedron. Two decagonal prisms with this property and associated with 2, 2′ are shown in figure 5.

The initial reference plane was chosen with the triangle tiling and hence has as its window a decagonal section through the triacontahedron perpendicular to the fivefold axis. An infinite system of parallel planes will arise, provided that we select a starting point which also belongs to a Fibonacci window associated with vectors say along the axis 2. The projection of the full Fibonacci window along the fivefold axis in $E_\perp$ by multiplication with $\cos(2,5) = 1/\sqrt{\tau+2}$ becomes $[2\tau^3/(\tau+2)]$⑤. The projection of its central subwindow for LL vertices equals the thickness $[2/(\tau+2)]$⑤ of the decagonal prism. We conclude that, among the parallel planes shifted along the infinite Fibonacci line in the direction 2, the reference plane and in fact any dense plane occurs at the LL vertices.

We summarize the *information obtained so far on parallel planes of vertex points*

$q_\parallel$ *in the tiling* $\mathcal{T}^{*(2F)}$, generated by Fibonacci lines along twofold axes: Starting from a dense reference plane, we generate an infinite set of parallel planes. They follow a Fibonacci spacing with perpendicular short and long distances $[2\tau/(\tau+2)]\textcircled{5} = 4.08$ Å and $[2\tau^2/(\tau+2)]\textcircled{5} = 6.60$ Å, fully in line with the STM observations of terraces. The dense planes occur at all LL vertices of the generating Fibonacci line. Other parallel planes in the set will have a lower density of vertex points. The string LLSLLSLSLL analysed in subsection 2.1 can now be converted into a sequence of parallel planes of varying density.

To complete the analysis of parallel planes, we must find out what fraction of all vertex points $q_\parallel \in \mathcal{T}^{*(2F)}$ is reached within this infinite sequence of planes.

2.5. Parallel planes are connected by Fibonacci lines

We wish to show that we can indeed reach from a fixed dense reference plane most vertex points $q_\parallel$ by shifts along Fibonacci lines. For this purpose we consider only those vertex points $q_\parallel$ which lie on at least one infinite Fibonacci line. From the window side we know that this is the case if $q_\perp$ is a point from any decagonal prism. There are six such prisms, and this motivates the definition of a new window:

Definition 2. *The decagonal prism* Xx *approximation: we analyse only those points* $q_\perp$ *of the triacontahedral window which belong to at least one decagonal prism—that is, to the union* $\cup_j^6 \text{prism}_j$. *We omit in this approximation the points* $q_\perp$ *from small parts of the triacontahedron close to its fivefold vertices; compare figure 5.*

The vertex points $q_\parallel$, with $q_\perp$ belonging to this new window, have the following properties:

Proposition 3. *Consider vertex points* $q_\parallel$ *in a plane parallel to a fixed dense TTT infinite reference plane. Among them there is a point on an infinite Fibonacci line which intersects (as a continuous line) the reference plane.*

Proof. Through any point coded in the decagonal prism approximation there runs at least one infinite Fibonacci line. If it intersects the reference plane the proof is complete. If it runs parallel to the reference plane, we can (proof omitted) in at most two parallel steps pass to another point with an intersecting Fibonacci line. □

Proposition 4. *If an infinite Fibonacci line intersects as a continuous line a TTT plane, it hits this plane in a vertex point.*

Proof. The points of the infinite reference plane form the vertices of the planar TTT subtiling with faces and the points of the non-parallel infinite Fibonacci line form the vertices of a linear subtiling with edges of the 3D tiling $\mathcal{T}^{*(2F)}$. Both subtilings are parts, hence their intersection is a vertex of the full tiling. □

The two propositions allow us to code, in $E_\perp$, planes of vertex points, parallel in $E_\parallel$ to a first dense reference plane perpendicular to 5, according to their intersections with Fibonacci lines along the axis 2 of figure 4:

Proposition 5. *Any vertex plane perpendicular to a fivefold axis has at least one point connected to the reference plane by an infinite Fibonacci line. Conversely, by following all non-parallel Fibonacci lines from the reference plane we reach any parallel vertex plane.*

We have shown that all vertex points $q_\parallel$ such that $q_\perp$ belongs to the Kepler Xx model appear in an infinite sequence of parallel planes in the order and spacing of a Fibonacci line. The analysis of the 1D Fibonacci system given in subsection 2.1 now applies to the 3D tiling. The stepwise generation in $E_\perp$ of the 1D Fibonacci system shown in figure 2 can now be converted into a stepwise generation in $E_\perp$ of parallel planes, enumerated by the integer N: starting at an LL vertex means starting at a dense plane. The value of the perpendicular coordinate $y_\perp$ yields the value of a coordinate $\eta\tau$⑤, $-1 \leqslant \eta \leqslant 1$, from the centre of the triacontahedron along the fivefold axis. The explicit relation is

$$\eta(N) = \frac{2\tau^{-1}}{\tau + 2} y_\perp(N). \tag{10}$$

In figure 6 we plot the projection of the triacontahedron together with the values of $y_\perp(N)$ connected by lines. Each value determines the height of a corresponding horizontal section of the triacontahedron. Since the point density in the corresponding plane of the tiling is proportional to the area of this section, figure 6 provides insight into the variation of this density from step to step.

Note that within the Fibonacci window we do not reach the highest absolute values of η. For the additional points in figure 6, see subsection 2.6.

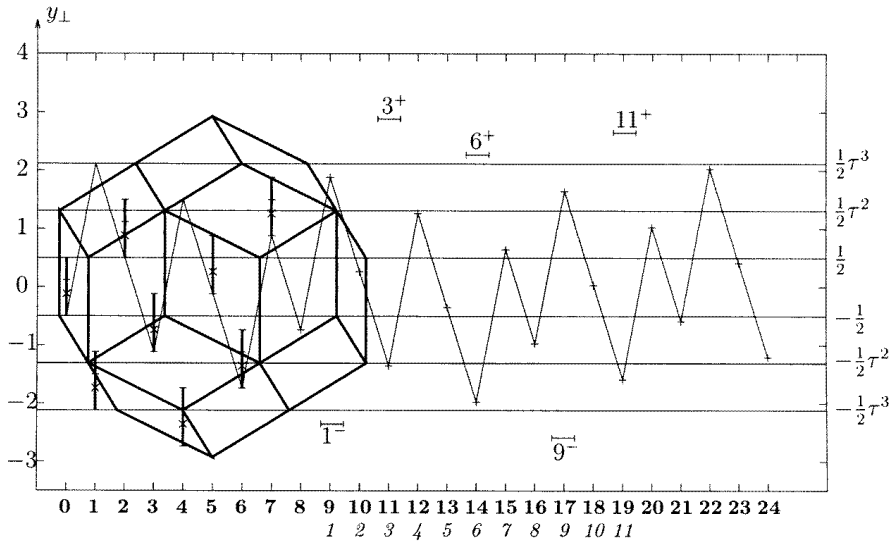

Figure 6. Vertical values of $y_\perp(N) \sim \eta(N)$, equation (10), determine horizontal sections in $E_\perp$ of the triacontahedron as windows for planes. The values are connected by lines and follow the Fibonacci coding. The total width of the vertical window is $[2\tau^2/(\tau + 2)]\tau$⑤. The triacontahedron has the vertical diameter 2τ⑤. The numbers in the second row assign planes corresponding to the terraces found in [15]. The bars labelled $1^-, 9^-, 3^+, 6^+, 11^+$ mark values of η for additional low-density planes of vertex points.

2.6. From planes to terraces at the surface

We have found in subsection 2.4, from the bulk model, sequences of planes with a spacing that agrees with the terrace spacing found in [15]. We now interpret terraces at the surface as particular planar terminations from the bulk tiling model. From figure 2 we have already identified a string in correspondence with the observed string of terraces. With the numbers

$1, \ldots, 11$ in the second horizontal row of figure 6, we now assign planes and values η_1 to eleven planes which correspond to the spacing of eleven high or low terraces found in [15]. The numbers follow the terraces in a direction into the bulk material.

The numbers η_1 given in table 1—see later—are not unique, but the appearance of the finite string puts narrow bounds on their range: maximal shifts upwards by $\Delta\eta = [2\tau^{-1}/(\tau+2)](2\tau-3)$ from $N = 9$ or downwards by $\Delta\eta = [2\tau^{-1}/(\tau+2)](-3\tau+5)$ from $N = 14$ are compatible with the appearance of the string, but of course give different values of the density and of the Patterson function.

As in the patch analysis given in [12], there appear additional vertex planes in $E_\parallel$ with a spacing scaled by τ^{-1} which do not yield terraces in the experiment. This narrow spacing cannot be coded by a single Fibonacci line. With respect to the triacontahedron in figure 5, it requires a vertical shift $\Delta\eta = 2\tau^2/(\tau+2)$ in $E_\perp$. This shift can be produced by the sum of two vectors of length τ② pointing along the axes 2 and 2′ in figure 2 respectively. The summed vector (not parallel to the fivefold axis) connects points in the triacontahedron only if the initial point obeys $\tau/(\tau+2) \leqslant |\eta| \leqslant \tau^2/(\tau+2)$. In the selection of points of figure 6, the values η of the corresponding five final points are denoted by $1^-, 3^+, 6^+, 9^-, 11^+$. The $\pm$ sign codes an additional vertex plane shifted in $E_\parallel$ by $2\tau^{-1}/(\tau+2)$ in units of τ⑤ above or below the plane with the fixed number. The positions of these planes agree with the patch analysis of [12]. All of these additional planes have very low densities of vertex points.

In subsection 3.2 we compute the exact model density of vertex points in the planes which decreases with the absolute value of η_1. From figure 6 it can be seen that the planes 3, 6, 9 in the string have the highest values of $|\eta_1|$ and hence the lowest density. In the experiment [15] these planes correspond to terraces of minimum measured planar size.

3. Clusters, pentagonal faces and cuts, and correlations in planes

We proceed to an analysis of the more detailed model structure within the planes. So far we have looked at planes occupied by vertex points from the tiling. The full set of atomic positions [4, 11] comprises more points in various classes. The repetition pattern and variation of the density for parallel planes found in section 2 is a general property of the tiling and applies to any set of atomic positions within planes perpendicular to a fivefold axis. If atomic positions of two different types appear within the same initial fixed plane, their repetition pattern and variation of density follow the same pattern as found for vertex points, but may propagate from different initial conditions. The relative density and the correlation of different types of atomic position sited within the same plane will then show *systematic variations* along a sequence of planes.

We consider in this section additional atomic positions from the Bergman clusters. The vertex positions of Bergman clusters on the tiling will produce points in parallel planes. This holds true in particular for top faces of Bergman clusters which run perpendicular to the chosen fivefold axis. They are of particular interest as candidates for the pentagons found in [15]. Upon comparing the height of 6.60 Å for the Bergman clusters with the lowest terrace spacing of 4.08 Å we already conclude that these clusters are *cut at quasicrystal surfaces*. A second larger type of pentagon arises from a top cut at the height of 4.08 Å through five vertices of the Bergman dodecahedra. In the full model [4, 11] of AlPdMn these top-face pentagons have central atoms in a lowered central position. Therefore these pentagon faces would produce at their centres the observed holes in the terraces [15]. We shall examine the correlation of both types of pentagon with vertex points of the tiling.

3.1. Three models for correlations of pentagons and vertex points

We analyse three significant types of plane perpendicular to a fivefold axis taken from the bulk model and explore the correlation within these planes.

(i) In the *first-model analysis* the vertex points of the tiling dominate the sequence of perpendicular planes, characterized by the values η_1 as before.

Consider the relation of the Bergman top pentagons with respect to these planes. As mentioned in the introduction, the centres of the Bergman dodecahedra take the positions of those (odd) points of the primitive P-lattice which are dropped when going from P to (2F). This has the consequence that the Bergman centres can be grouped into shifted planes perpendicular to a fivefold axis. The planar densities of Bergman clusters in these planes must follow the same rules, and have the same minima and maxima as are given for vertex positions in subsections 2.4 and 3.2.

The height of the Bergman dodecahedra is such that a fivefold vector from the plane to the centre, passing through a pentagonal face, has the length and direction of a typical vector $e_{5\|}$; compare figure 7. With the chosen enumeration of terraces we follow them in the direction of the vector $e_{1\|}$, *in the direction* of the fivefold axis in figure 4. Now we look for Bergman clusters with a centre displaced below and a top pentagon within a fixed plane of vertex points.

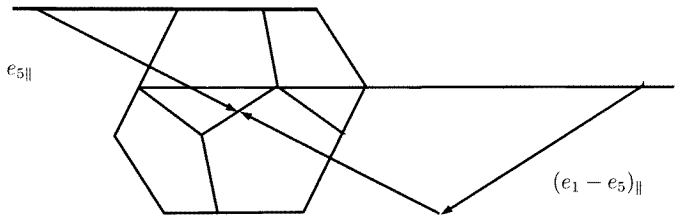

Figure 7. A Bergman dodecahedron touches a top pentagon from below a plane of vertex points marked by the top horizontal line. The vector $e_{1\|}$ points *downwards*. A typical vector downwards from the plane to the Bergman centre is $e_{5\|}$. A vector like $(e_1 - e_5)_\| - e_{5\|}$ runs from a planar pentagonal top cut through the dodecahedron, marked by the lower horizontal line, to the Bergman centre.

Transforming the vector $e_{5\|}$ from $E_\|$ to $E_\perp$—compare subsection 2.2—one finds the coding points for all centres of the Bergman dodecahedra displaced by $e_{5\perp}$ *against the direction of the axis* 5 of figure 5, and hence downwards in figure 5, from the plane coding the vertex points. So the planes with a corresponding *downwards shift* $\Delta\eta = 1/(\tau + 2)$ form another Fibonacci sequence that codes the Bergman centres. The shifted values η_2 for this sequence are given in the second column of table 1—see later. In figure 8 we show the two values η_1, η_2 as functions of $N = 0, \ldots, 24$. If the vertical shift from the crosses to the circles equals $\Delta\eta = 1/(\tau + 2)$, the Bergman top pentagons touch the vertex plane from below. This holds true except for the planes $N = 6, 11, 14, 19$; see figure 8. In the Fibonacci sequence of planes of vertex points this corresponds to an LS vertex, but in the planes of Bergman faces it corresponds to an SL vertex. Therefore no Bergman top faces can appear in these planes of vertex points. In the string of planes $9, \ldots, 19 \rightarrow 1, \ldots, 11$ this would occur at the planes $11, 14, 19 \rightarrow 3, 6, 11$. These planes carry instead the larger Bergman top-cut pentagons; see model (iii) below.

Figures 8 and 9 demonstrate that planes formed from atomic positions of different types (vertex points or pentagon centres) follow the same Fibonacci propagation law. Due to systematic shifts in the parameter η for different types, the corresponding densities, which

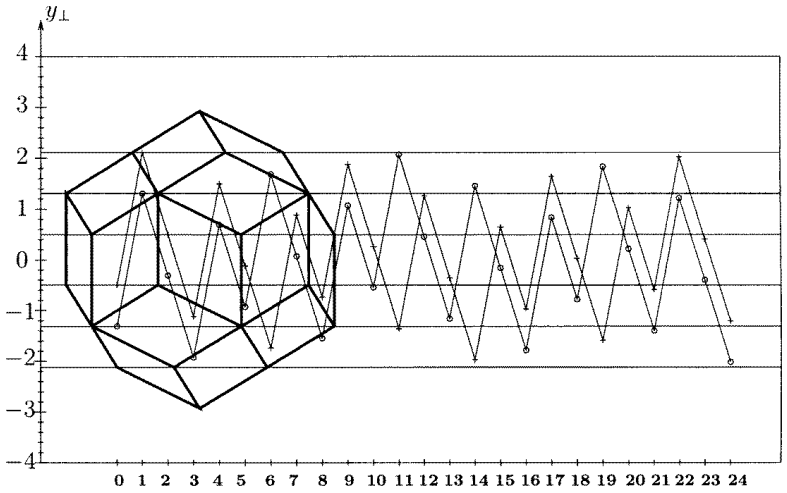

Figure 8. The values $y_\perp(N) \sim \eta(N)$ for $N = 0, \ldots, 24$ in model (i) determine horizontal sections of the triacontahedron as windows for planes of vertex points (η_1, crosses) or of centres for Bergman top pentagons (η_2, circles).

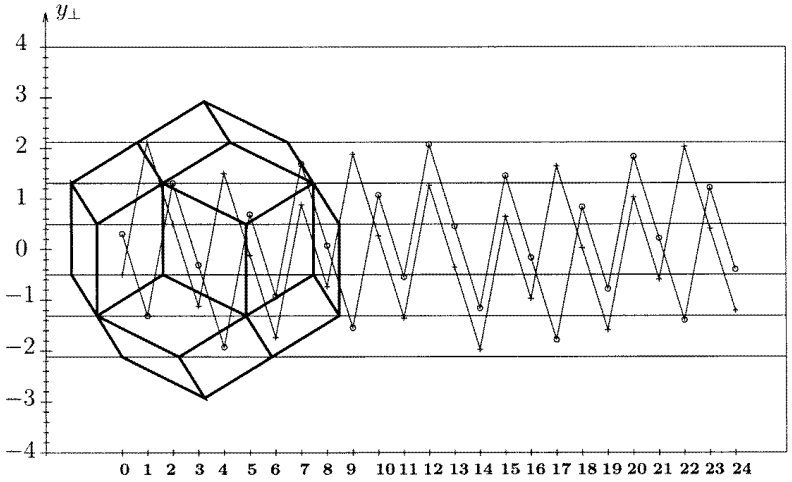

Figure 9. The values $y_\perp(N) \sim \eta(N)$ for $N = 0, \ldots, 24$ in model (ii) determine horizontal sections of the triacontahedron as windows for planes of centres for Bergman top pentagons (η_1, crosses) or of vertex points (η_3, circles).

are functions of this parameter, propagate differently even for atomic positions of different types within the same initial plane.

(ii) In the *second-model analysis* of the planes determined by η_1 we assume that they are dominated by top pentagons of Bergman dodecahedra located below the plane; compare figure 9. The additional presence of vertex points on these planes is now coded by a *positive shift* $\Delta\eta = 1/(\tau + 2)$. In table 1, later, we give the new values η_3 for these vertex planes and show them in figure 9. Additional vertex points appear except in the selected planes $9, 17 \to 1, 9$.

(iii) In the *third-model analysis* we assume that the planes determined by η_1 are dominated by pentagons, scaled by τ and corresponding to top cuts through Bergman dodecahedra below the plane. A typical vector from the plane for this cut to the centre of the Bergman cluster in the notation of subsection 2.2 is $(-e_{5\|} + e_{1\|}) - e_{5\|}$ indicated in figure 7. The edge size ② = 4.78 Å of the pentagons would be in line with the holes observed in [15], and it would also lead to a central hole. Again we ask about the presence of additional vertex points. From the positions of these pentagons relative to the vertex planes as shown in figure 7 we deduce in $E_\perp$ a shift $\Delta\eta = (2\tau + 1)/(\tau + 2)$. At $N = 0$ this shift modulo the window size becomes $-1/(\tau + 2)$ which then generates the values η_3 given in table 1, later, and shown in figure 9. Vertex points can occur only if the relative shift from crosses to circles is $\Delta\eta = \eta_3 - \eta_1 = (2\tau + 1)/(\tau + 2)$. This happens only in the selected planes $9, 17 \to 1, 9$; otherwise there are no vertex points within these planes. A further shift analysis shows that any plane containing Bergman top pentagons cannot contain Bergman cut pentagons and vice versa. In model (iii) there appear Bergman top-cut pentagons in the densest planes. A closer inspection shows that these pentagons share vertices and form an almost connected graph.

The three model cases considered yield three interpretations of bulk planes as terminations for the terraces observed in [15], all in line with the relative spacing. In cases (i), (ii) the planes carry vertex points or pentagons corresponding to the faces of Bergman dodecahedra. In case (iii) the planes carry the larger cut pentagons and almost no vertex points.

3.2. Planar density of atomic positions

We compute the exact area $F(\eta)$ of a planar section of the triacontahedron as a function of η, $-1 \leqslant \eta \leqslant 1$. This function is proportional to the exact density of vertex points $D(\eta)$ in the plane coded by this section. The result is

$$0 \leqslant |\eta| \leqslant \frac{\tau^{-1}}{\tau+2}: \qquad F(\eta) = (\tau+2)^{-3/2}\,[10\tau] \tag{11a}$$

$$\frac{\tau^{-1}}{\tau+2} \leqslant |\eta| \leqslant \frac{\tau}{\tau+2}: \qquad F(\eta) = (\tau+2)^{-3/2}\left[10\tau - 5\frac{(\tau+2)^2}{\tau}\left(|\eta| - \frac{\tau^{-1}}{\tau+2}\right)^2\right] \tag{11b}$$

$$\frac{\tau}{\tau+2} \leqslant |\eta| \leqslant \frac{\tau^2}{\tau+2}: \qquad F(\eta) = (\tau+2)^{-3/2}\left[10 + 5\frac{(\tau+2)^2}{\tau}\left(\frac{\tau^2}{\tau+2} - |\eta|\right)^2 - 5(\tau+2)^2\left(|\eta| - \frac{\tau}{\tau+2}\right)^2\right] \tag{11c}$$

$$\frac{\tau^2}{\tau+2} \leqslant |\eta| \leqslant 1: \qquad F(\eta) = (\tau+2)^{-3/2}\left[5(\tau+2)^2(1-|\eta|)^2\right]. \tag{11d}$$

The function $F(\eta)$ is plotted in figure 10. The maximum is $F(0) = 10\tau(\tau+2)^{-3/2} = 2.3511$; the maximum value of η for the Fibonacci sequence of planes is

$$|\eta| = \tau^2(\tau+2)^{-1} = 0.7236. \tag{12}$$

These values are marked by vertical and horizontal lines in figure 10.

The density can be converted into the absolute density of vertex points by considering the densest planes with a triangle pattern and its vertices: in the triangle pattern, each triangle contributes, because of the sum $\frac{1}{2}2\pi$ of its angles, a weight $\frac{1}{2}$ to the number of vertex points. In terms of the short-edge length s, the areas f_1, f_2 and relative frequencies ν_1, ν_2 of the large and small triangles are

$$f_1 = s^2\frac{\tau}{4}\sqrt{\tau+2} \qquad f_2 = \tau^{-1}f_1 \qquad \nu_2 = \tau^{-1}\nu_1. \tag{13}$$

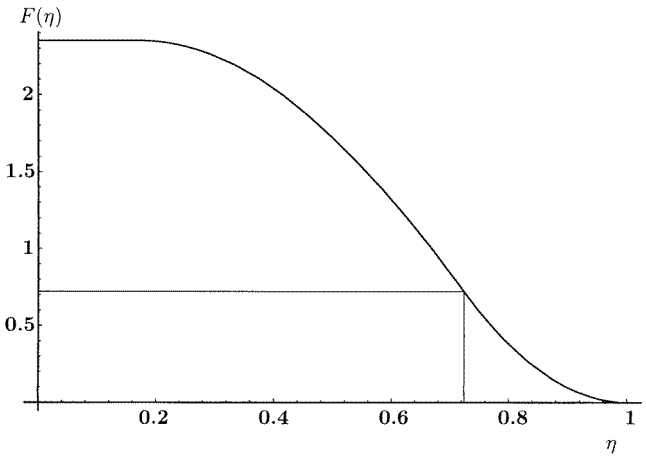

Figure 10. The function $F(|\eta|)$ for a plane fixed by $\eta \geqslant 0$ is, in $E_\perp$, the area of a planar section of the triacontahedron. The horizontal line marks the lowest value of F, the vertical line the highest value of $|\eta|$ in a Fibonacci sequence of planes. In $E_\parallel$, $F(|\eta|)$ is proportional to the density of points or pentagon centres within a plane.

These expressions yield for the *density of vertex points* (number of vertices per unit area) the value

$$D(0) = \frac{1}{2f_1}\frac{\tau^3}{\tau+2} = s^{-2}\frac{2\tau^2}{(\tau+2)^{3/2}}. \tag{14}$$

In the present model we put for the short-edge length $s = \tau ② = \tau(2/\sqrt{\tau+2})⑤$ and $⑤ = 4.56$ Å, equation (1), to obtain the model value

$$D_{\max,(\mathrm{i})} = D(0) = 12.6 \times 10^{-3}\ \text{Å}^{-2}. \tag{15}$$

The density of vertex points in a plane for fixed η is now computed as

$$D(\eta) = D(0)\frac{F(\eta)}{F(0)}. \tag{16}$$

The lowest density in a Fibonacci sequence of planes from equations (14), (15) is

$$D_{\min} = \frac{1}{2\tau}D(0) = 0.3090D(0). \tag{17}$$

These values of the density refer to vertex positions in the tiling. All other atomic positions on the tiles will of course lead to other specific atomic densities and correlations.

The maximum density of vertex points, associated with model (i), is given in equation (16). The same maximal density applies to the centres of Bergman top faces in model (ii). Each pentagon contributes five vertex positions which would yield a factor of 5 for the pentagon vertex density. For model (iii) with the larger pentagons, the maximum density of centres is still the same. For the density of pentagon vertices one should not multiply by a factor of 5: it turns out that these larger pentagons in a dense plane can share vertices. An exact computation of the maximum density for the vertices of large pentagons yields (proof omitted)

$$D_{\max,(\mathrm{iii})} = \frac{7\tau+4}{\tau^3}D_{\max,(\mathrm{i})} = 3.6180D_{\max,(\mathrm{i})}. \tag{18}$$

From the density we can compute the average distance by comparison for example with a tiling by equilateral triangles. For such a tiling, the density of points is related to the edge length t by

$$D_3(t) = t^{-2}2/\sqrt{3}. \tag{19}$$

If we equate this density with the expression (15) found for the dense vertex planes, we obtain an equivalent distance $t_{eq} = 9.5$ Å.

In columns 5–7 of table 1 we give F for the three values of η. Note that, in view of the three models discussed in subsection 3.1, the three values of F in a row do not always refer to the same plane.

Table 1. The values η_1, η_2, η_3 as functions of $N = 0, \ldots, 24$ code inside the triacontahedron Fibonacci sequences of planes perpendicular to a fivefold axis. These values are associated alternatively with vertex points, pentagonal faces, and cuts of Bergman dodecahedra. Columns 5–7 give the values of $F(\eta_i)$, equal to the area of planar sections through the triacontahedron and proportional to the relative density of points. The rows $9, \ldots, 19$ correspond to the terraces $1, \ldots, 11$ of [15].

N	η_1	η_2	η_3	$F(\eta_1)$	$F(\eta_2)$	$F(\eta_3)$
0	−0.1708	−0.4472	0.1056	2.3511	1.9021	2.3511
1	0.7236	0.4472	−0.4472	0.7265	1.9021	1.9021
2	0.1708	−0.1056	0.4472	2.3511	2.3511	1.9021
3	−0.3820	−0.6584	−0.1056	2.0891	1.0541	2.3511
4	0.5125	0.2361	−0.6584	1.6746	2.3261	1.0541
5	−0.0403	−0.3167	0.2361	2.3511	2.2260	2.3261
6	−0.5931	0.5777	−0.3167	1.3507	1.4162	2.2260
7	0.3013	0.0249	0.5777	2.2510	2.3511	1.4162
8	−0.2515	−0.5279	0.0249	2.3129	1.6164	2.3511
9	0.6430	0.3666	−0.5279	1.1269	2.1259	1.6164
10	0.0902	−0.1862	0.3666	2.3511	2.3497	2.1259
11	−0.4626	0.7082	−0.1862	1.8512	0.8067	2.3497
12	0.4318	0.1554	0.7082	1.9508	2.3511	0.8067
13	−0.1210	−0.3974	0.1554	2.3511	2.0495	2.3511
14	−0.6738	0.4971	−0.3974	0.9796	1.7311	2.0495
15	0.2207	−0.0557	0.4971	2.3365	2.3511	1.7311
16	−0.3321	−0.6085	−0.0557	2.1982	1.2835	2.3511
17	0.5623	0.2859	−0.6085	1.4800	2.2733	1.2835
18	0.0095	−0.2669	0.2859	2.3511	2.2969	2.2733
19	−0.5433	0.6276	−0.2669	1.5565	1.1980	2.2969
20	0.3512	0.0748	0.6276	2.1600	2.3511	1.1980
21	−0.2016	−0.4780	0.0748	2.3456	1.7986	2.3511
22	0.6928	0.4164	−0.4780	0.8851	1.9966	1.7986
23	0.1400	−0.1364	0.4164	2.3511	2.3511	1.9966
24	−0.4128	−0.6892	−0.1364	2.0070	0.9033	2.3511

The three models (i), (ii), (iii) given in subsection 3.1 yield different density values F. In model (i), the density of vertex points and centres of Bergman top faces is given by $F(\eta_1)$ and, with exceptions, by $F(\eta_2)$. In the plane $16 \to 8$, the density of Bergman faces becomes $D = 6.8 \times 10^{-3}$ Å^{-2}. In model (ii), the density of Bergman top faces and vertex points is given by $F(\eta_1)$ and, with exceptions, by $F(\eta_3)$. In model (iii), the density of Bergman top cuts is again given by $F(\eta_1)$.

The density of pentagonal holes in the experimental data [15] has approximately [12] the value $D = 4.2 \times 10^{-3}$ Å^{-2}. This value would favour model (i) with Bergman top faces in planes dominated by vertex points.

3.3. Patterson analysis in planes

Consider the general Patterson function $P(x_\parallel)$ of a quasiperiodic point set with a window W at each point of the lattice Λ. Let $v_\parallel$ be a shift vector projected from a lattice vector v. Let $\chi(x_\perp)$ be the characteristic function of the window W for the lattice points projected to $E_\perp$.

Proposition 6. *The Patterson function in $E_\parallel$ at $x_\parallel = x - x_\perp$ is given by*

$$P^{\text{total}}(x_\parallel) = \sum_{v\in\Lambda} \delta(x_\parallel - v_\parallel) \int_{\text{W}} \chi(x_\perp)\chi(x_\perp - v_\perp)\,\mathrm{d}x_\perp = \sum_{v\in\Lambda} \delta(x_\parallel - v_\parallel) P(v_\perp). \tag{20}$$

We shall put $P(v_\parallel) = P(v_\perp)$. A Patterson analysis within a plane perpendicular to the fivefold axis 5 with a fixed shift vector $v_\parallel$ parallel to this plane involves the following notions for $E_\perp$: consider the corresponding planar section of the triacontahedron with an intersection at $\eta\tau$⑤ along the fivefold axis 5. The values of η for the eleven selected planes are given in table 1 both for the vertex points and for the centres of Bergman dodecahedra touching the vertex plane from below. The area of the planar section is proportional to the density $D(\eta)$ of vertex points. The terraces 2, 5, 10 in this interpretation are dense vertex planes. The terraces 2 and 7 have the highest, and the terrace 6 the lowest density of Bergman faces.

The Patterson function from proposition 4 is computed as follows: shift the planar section by the vector $v_\perp$ parallel to itself. Compute the area of the intersection of the shifted and unshifted section. This area is proportional to the value of the Patterson function in $E_\parallel$ at the point $v_\parallel$. The value of $P(0)$ is proportional to the density of points. We may also normalize by plotting $P(v_\parallel)/P(0)$.

In a *circle approximation* we proceed as follows.

We use the exact area $F(\eta)$ of a planar section of the triacontahedron as a function of η.

For any fixed value of η we compute the radius $r(\eta)$ of a circle with the same area as the section; hence,

$$r(\eta) := \sqrt{\pi^{-1}F(\eta)}. \tag{21}$$

This amounts to replacing the triacontahedron by a rotational surface whose circular areas (and hence density values) for any η are equal to those of the triacontahedron. Then we approximate

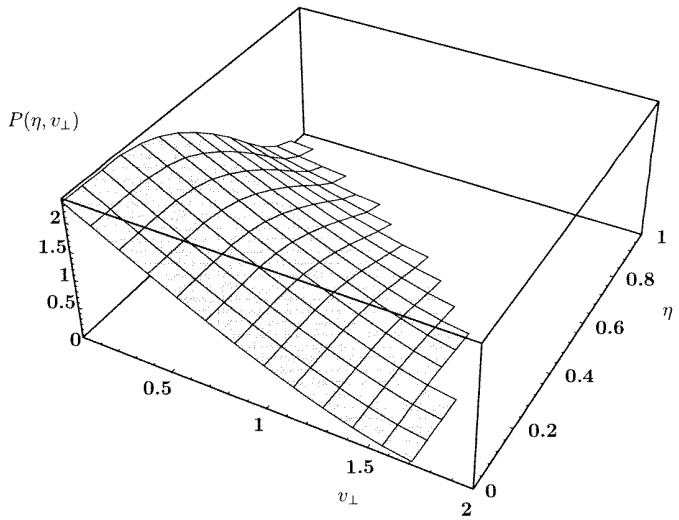

Figure 11. The Patterson function $P(\eta, v_\perp)$. For $v_\perp = 0$ it reduces to $F(\eta)$.

the Patterson function by using these circles instead of the polygonal sections as functions of η. In this approximation, the Patterson function only depends on $|v_\perp|$.

The Patterson function P has a smooth behaviour in terms of the two variables η and $v_\perp$. This expression is shown in figure 11. For $v_\perp = 0$ it reduces to the function $F(\eta)$, and for $v_\perp = 2r(0)$ it must go to zero.

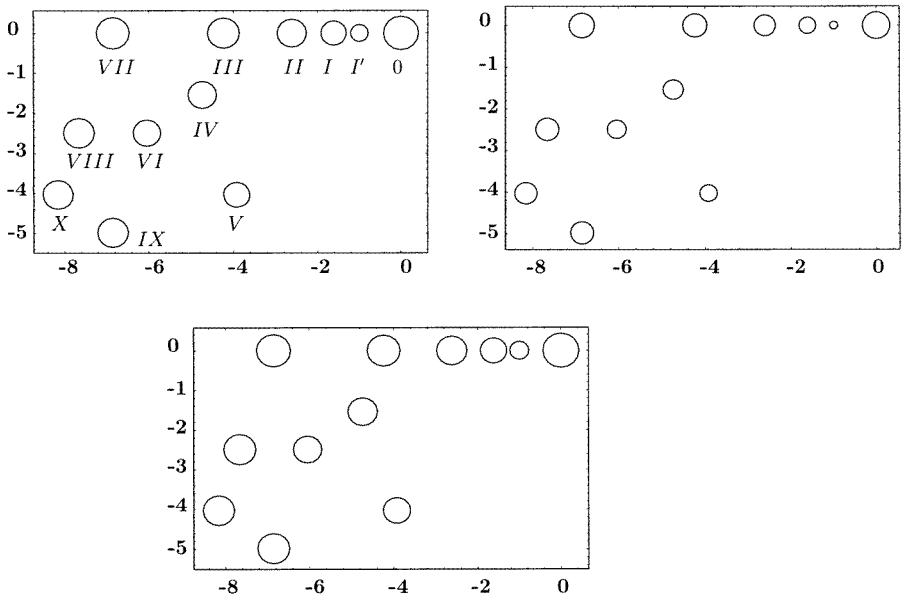

Figure 12. The Patterson function P corresponding to the values $N = 16 \rightarrow 8$ for the values η_1, η_2, η_3 from table 1, represented by the areas of circles in a plane. The upper right-hand circle stands for 0: $v_\parallel = 0$; the first point I′ to its left is at a distance $|v_\parallel| = 7.78$ Å; the others are labelled by Roman numerals I, . . . , X in correspondence with [15].

For the plane number $16 \rightarrow 8$, we give in figure 12 the values of the Patterson function P for η_1, η_2, η_3, represented by areas of circles, as functions of the eleven points $v_\parallel$ selected in a plane as in [15].

In figure 13 we present the same values as functions of the ten Roman numerals which label the peak positions $v_\parallel$. It can be seen that $P(\eta_2)$ yields the lowest density and the strongest relative variation, and $P(\eta_1)$ and $P(\eta_3)$ are very similar, but the latter yields the highest density.

We can now compare the three different models (i), (ii), (iii) of the terrace structure given in subsection 3.1 in terms of the Patterson data for terrace 8. Model (i) yields the lowest value of the Patterson data for the Bergman top faces, along with a larger value for the vertex points. Models (ii) and (iii) give the same larger values of the Patterson function for the small or the large top pentagons, but differ as regards the presence or absence of vertex points (respectively). All three models are compatible with the qualitative set of experimental Patterson data [15].

4. Conclusions

We analyse a tiling model for the surface structure of i-$Al_{68}Pd_{23}Mn_9$ quasicrystals perpendicular to a fivefold axis. The surfaces are interpreted as terminations in atomic planes from the bulk tiling model decorated by Bergman clusters. The model is analysed in a window

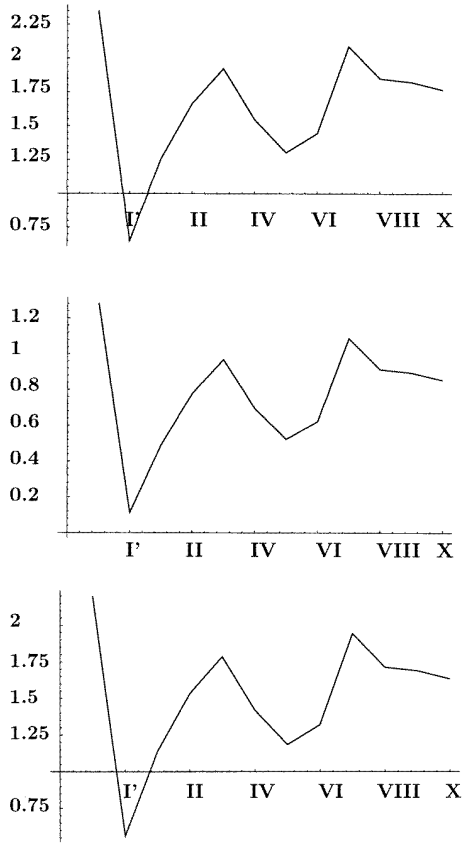

Figure 13. The Patterson function P as in figure 12 as a function of the Roman numerals I′, I, . . . , X for the three values η_1, η_2, η_3 from top to bottom.

approach. The quasiperiodic relations between planes occupied by atoms are rigorously and quantitatively derived from the bulk model. Sequences of planes are shown to be generated and connected by infinite Fibonacci lines running through the tiling. Both the density and the Patterson data for different types of atomic position are computed in closed form and shown to vary strongly between the planes.

In the planes, we consider vertex positions of the tiling and pentagonal positions arising from faces or top cuts through the Bergman clusters. Changes of their correlation between the planes are analysed in three alternative models. The pentagonal holes observed in [15] admit an interpretation in terms of these pentagons. If they arise from the Bergman top pentagons, their observed larger size must reflect a local reconstruction of the surface. If they arise from the Bergman top-cut pentagons, they agree with the observed size.

The geometries, the spacings, the densities, and the Patterson functions are computed from the bulk model. The sequence and spacing of terraces and the available Patterson data from [15] are well reproduced. The observed Fibonacci string of planes yields information on the density of atomic positions. The observed size of the terraces shows some correlation with the model structure in the planes.

More detailed experimental studies of the terrace structure in icosahedral quasicrystals are suggested.

Acknowledgment

The authors would like to thank Tobias Kramer for substantial help in the computation and presentation of data.

References

[1] Baake M, Kramer P, Schlottmann M and Zeidler D 1990 *Int. J. Mod. Phys.* B **4** 2217
[2] de Boissieu M, Stephens P, Boudard M, Janot C, Chapman D L and Audier M 1994 *J. Phys.: Condens. Matter* **6** 10 725
[3] Ebert Ph, Yue F and Urban K 1998 *Phys. Rev.* B **57** 2821
[4] Elser V 1996 *Phil. Mag.* B **73** 641
[5] Gierer M, Van Hove M A, Goldman A I, Shen Z, Chang S-L, Jenks C-M, Zhang C-M and Thiel P A 1997 *Phys. Rev. Lett.* **78** 467
[6] Gierer M, Van Hove M A, Goldman A I, Shen Z, Chang S-L, Pinhero P J, Jenks C M, Anderegg J W, Zhang C-M and Thiel P A 1998 *Phys. Rev.* B **57** 7628
[7] Katz A and Gratias D 1995 *Proc. 5th Int. Conf. on Quasicrystals* ed C Janot and R Mosseri (Singapore: World Scientific) pp 164–7
[8] Kepler J 1619 *Harmonice Mundi* (German Transl. Caspar M 1973 *Weltharmonik* (Munich: Oldenbourg) p 74)
[9] Kramer P and Neri R 1984 *Acta Crystallogr.* A **40** 580
[10] Kramer P, Papadopolos Z and Zeidler D 1991 *Symmetries of Icosahedral Quasicrystals (Symmetry in Science vol 5)* ed B Gruber, L C Biedenharn and H D Doebner (New York: Plenum) pp 395–427
[11] Kramer P, Papadopolos Z and Liebermeister W 1998 *Proc. 6th Int. Conf. on Quasicrystals* ed S Takeuchi and T Fujiwara (Singapore: World Scientific) pp 71–6
Kramer P, Papadopolos Z and Liebermeister W (ed) 1997 Atomic positions for the icosahedral F-phase tiling *Proc. Aperiodic '97*
[12] Kasner G, Papadopolos Z, Kramer P and Bürgler D E 1999 submitted
[13] Papadopolos Z, Kramer P and Zeidler D 1993 *J. Non-Cryst. Solids* **153+154** 215
[14] Moody R V 1997 Meyer sets and their duals *The Mathematics of Long-Range Aperiodic Order* ed R V Moody (Dordrecht: Kluwer) pp 403–41
[15] Schaub T M, Bürgler D E, Güntherodt H-J and Suck J B 1994 *Phys. Rev. Lett.* **73** 1255
Schaub T M, Bürgler D E, Güntherodt H-J, Suck J B and Audier M 1995 *Appl. Phys.* A **61** 491